Reactive melt crosslinking of cellulose nanocrystals/poly(ε-caprolactone) for heat-shrinkable network

Composites: Part A 163 (2022) 107166

Contents lists available at ScienceDirect

Composites Part A

journal homepage: www.elsevier.com/locate/compositesa

Reactive melt crosslinking of cellulose nanocrystals/poly(ε-caprolactone) for heat-shrinkable network

Angelica Avella [a], Alexander Idström [b], Rosica Mincheva [c], Koyuru Nakayama [b,d], Lars Evenäs [b,d], Jean-Marie Raquez [c], Giada Lo Re [a,d,*]

[a] Department of Industrial and Materials Science, Chalmers University of Technology, 41258 Gothenburg, Sweden
[b] Department of Chemistry and Chemical Engineering, Chalmers University of Technology, 41258 Gothenburg, Sweden
[c] Laboratory of Polymeric and Composite Materials, University of Mons (UMONS), 7000 Mons, Belgium
[d] Wallenberg Wood Science Centre (WWSC), Chalmers University of Technology, 41296 Gothenburg, Sweden

ARTICLE INFO

Keywords:
Biocomposite
Cellulose
Creep
Reactive melt processing

ABSTRACT

Focusing on the challenge of non-biodegradable plastics replacement, we propose a design for peroxide-initiated crosslinking of biodegradable poly(ε-caprolactone) (PCL) and renewable cellulose nanocrystals (CNCs) bionanocomposites. An industrially scalable water-assisted reactive melt-processing (REx) is studied to explore the hypothesis of synergy between simultaneous effects of water on improving CNC dispersion and boosting PCL branching/crosslinking. We demonstrate that the melt processing control enables the preparation of targeted thermoplastic/thermoset bionanocomposites with gel content up to ≈ 40 %, identified as the limit of their melt-processability. Structural characterization reveals that ≈ 70 wt% of the initial CNC content is irreversibly incorporated in a percolating network, enhancing the crosslinked bionanocomposites properties. The bionanocomposites' complex viscosity and elastic character increase with the gel content, thus improving PCL melt performance. Furthermore, the irreversible entrapment of CNCs in the 3D percolating network provides heat-shrinkability, indicating a potential of the reacted bionanocomposites for heat-triggered shape-memory.

1. Introduction

The increasing presence of plastic waste in landfills and marine environment plays a key role in the growing of environmental awareness, questioning the use of conventional plastics according to the product lifespan, *e.g.* single-use applications. More than 50 % of globally produced plastic until 2015 (8300 million metric tons) has been discarded in the environment [1]. Of the 300 Mt of plastic waste in 2015, the 40 % is packaging, mainly composed of non-biodegradable thermoplastics [1]. Therefore, the environmental impact of conventional plastics can be mitigated by their replacement with biodegradable materials. The current production of biodegradable thermoplastics still represents less than 1 % of the global plastics market [2]. Their relatively high cost, followed by challenges in processability and reliability of thermomechanical performance further limit their spreading in the manufacturing sector [3]. Actions to improve the knowledge and competence on biodegradable thermoplastics in support of their industrial uptake contribute to the achievement of the United Nations sustainable development goals [4].

The biodegradable poly(ε-caprolactone) (PCL) represents a promising alternative to the widely used low-density polyethylene, due to their similar mechanical properties [5]. Our work aims to contribute in improving its processability, performance and bio-based content, by producing biodegradable lignocellulosic composites [6]. Radical crosslinking has shown to improve PCL rheological and thermomechanical properties [7–10], even enhancing PCL biodegradability via molecular weight distribution broadening [11]. Cellulose nanocrystals (CNCs) are becoming attractive for large-scale melt processing due to their high stiffness (Young's modulus 100–200 GPa [12]), and recent commercial availability. A full exploitation of CNC nanostructure would imply a change of the bionanocomposite bulk at the nanoscale, both in the solid and in the melt state. The targeted "nano-effect" can be achieved by homogeneous CNC dispersion in the thermoplastic matrix [13] and a strong interfacial adhesion, enabling an efficient stress transfer [14]. However, the significant presence of hydroxyl groups on CNC surfaces promotes irreversible agglomeration that hinders the "nano-effect" [15].

* Corresponding author at: Rännvägen 2A, 41258 Gothenburg, Sweden.
E-mail addresses: avella@chalmers.se (A. Avella), idstrom@chalmers.se (A. Idström), rosica.mincheva@umons.ac.be (R. Mincheva), koyuru@chalmers.se (K. Nakayama), lars.evenas@chalmers.se (L. Evenäs), jean-marie.raquez@umons.ac.be (J.-M. Raquez), giadal@chalmers.se (G. Lo Re).

https://doi.org/10.1016/j.compositesa.2022.107166
Received 10 July 2022; Received in revised form 17 August 2022; Accepted 18 August 2022
Available online 22 August 2022

As the agglomeration becomes irreversible already upon drying (hornification) [16], celluloses have been successfully dispersed into polyesters by water-assisted approaches [17], enabling more effective reinforcement, mainly when hydrolytic degradation of the matrices is minimal, such as in PCL [5,18–20]. In addition, this wet-feeding from water dispersion circumvents the potential dangers of handling nanoparticles, leading to greener safer processing and easier upscaling.

Reactive melt processing (REx) provides the benefits of a simultaneous compatibilization/compounding/shaping process without any toxic solvent, thus resulting in a cost-effective sustainable method with potential to ease the industrial uptake [3,21]. Few studies have focused only on the effect of peroxide for REx of cellulose/polyesters biocomposites. Crosslinking of polylactic acid (PLA) in presence of CNCs or nanofibrils has been reported after spraying dicumyl peroxide (DCP)/acetone solution on PLA pellets [22,23]. Wei et al. produced biocomposites of polyhydroxybutyrate (PHB) or poly(hydroxy-butyrate-co-hydroxyvalerate) (PHBV) with cellulose fibers following a similar spraying procedure from DCP/acetone solution [24,25]. Zheng et al. [26] demonstrated that peroxide-initiated in-situ grafting of PHBV on CNCs favored their dispersion, so improving biocomposites strength, when compared to direct melt blending or the use of a coupling agent. These biocomposites showed enhanced rheological and mechanical properties by REx-induced crosslinking and improved surface adhesion between cellulose and the polyesters. Dynamic rheological measurements indicated that branching/crosslinking led to an increase in melt viscosity (up to two orders of magnitude) and elasticity [23,25].

We developed a novel simultaneous green REx and sustainable bionanocomposites production grounded on the hypothesis of a synergy between water-assisted PCL crosslinking [27] and CNC wet-feeding. Therefore, water was exploited for the first time in two simultaneous key roles: booster of radical crosslinking and dispersant for CNCs. The REx design targeted a gel content ≈ 40 % to preserve melt processability of the bionanocomposites. We unraveled the relationship between melt crosslinking, molecular structure, and physical properties of synergic thermoplastic/thermoset CNC/PCL network which also disclosed heat-shrinking. Our results demonstrate the relevance of industrially scalable REx designs to improve in a single step not only the melt processability and the performance of novel sustainable biocomposites, but also to broaden their applications.

In the context of heat-shrinkable temperature sensors and actuators, or single-use films and tubing for packaging of food, bottles packs and electronics [28,29], our heat-triggered bionanocomposite is a sustainable alternative to currently used polymers such as polyethylene and polyvinyl chloride (PVC). Our bionanocomposite provides the advantages of lower melting point/heat-triggering temperature, absence of harmful substances, *i.e.* PVC additives, increased bio-based content and potential biodegradability. Aware of the crucial aspect of assessing the end-of-life of biocomposites due to the possible controversial effect of crosslinking and CNCs on the biodegradability and recyclability of the materials, our promising results motivate future investigations and validation on these end-of-life options.

2. Experimental

2.1. Materials

PCL Capa6506 in powder form was purchased from Ingevity, UK (number average molecular weight $\overline{M_n} \approx 50{,}000$ g·mol^{-1}, melt flow rate of 7.9–5.9 g/10 min at 190 °C/2.16 kg). PCL-diol (AcrossOrganics, $\overline{M_n} = 2{,}000$ g·mol^{-1}) was used after drying at 60 °C under reduced pressure for 48 h. Water dispersion (8 wt% solid content) of sulphuric acid-hydrolyzed CNC was purchased from CelluForce, Canada. The CNC has average length of 301 ± 110 nm and diameter of 6 ± 3 nm, consequently an aspect ratio of ≈ 50 (Figure S1 in Supporting Information (SI)) [30]. Benzoyl peroxide (BPO) (Luperox A75) and 2,2,6,6-Tetramethylpiperidine-1-oxyl (TEMPO) were purchased from Sigma-Aldrich and were used without further purification. Dichloromethane (DCM) and chloroform were purchased from VWR International with purity higher than 99.5 %.

2.2. Reactive melt processing

PCL was manually premixed with CNC water dispersion to obtain bionanocomposites with PCL:CNC ratio as 90:10 dry wt.%. The final amount of CNC was targeted at 10 wt% of the total bionanocomposites mass, well above percolation threshold to ensure CNC network formation taking into account the challenges of CNCs individualization in melt compounding and the possible inclusion of redispersing agents such as polyethylene glycol in CelluForce CNC [31]. Effective stiffening has been previously achieved even in melt processing [32] and even in solvent casted [33] poly(ε-caprolactone) (PCL) bionanocomposites at a CNC content ≈ 5 times the percolation threshold (Equation S1), CNC morphology and other details in SI.

Different BPO amounts (0 to 1 wt% of PCL content) were added to the PCL/CNC paste, which was melt processed in an internal mixer Brabender® AEV 330 (50 cm^3) with counter-rotating screws. The water-assisted melt processing was carried out at 120 °C to enable water evaporation [5] and ensure BPO melting (BPO onset and melting temperatures ≈ 98 and 103 °C, respectively [34]). The overall processing time was 15 min, in particular feeding for ≈ 5 min at 30 rpm, then 10 min at 60 rpm. The processing time took into consideration the BPO half-life (≈ 3 min at 120 °C [35]). PCL references were produced according to the same method, by premixing PCL with the equivalent amount of deionized water present in the CNC dispersion and 0.5 or 1 wt % BPO. A reference was also prepared with 3 wt% BPO, maintaining the same ratio of water and PCL but halving the processed mass in the internal mixer. The reacted bionanocomposites and PCL references have been coded as PCL-CNC-xL and PCL-xL, respectively, where the value "x" indicates the wt.% of peroxide (Luperox) used during REx (Table S1). All the produced materials, except for PCL-3L, were shaped into squared films of 1 mm thickness using a compression molder Buscher-Guyer KHL 100 at 120 °C for 3 min at 40 bar and 1 min at 500 bar, followed by quenching to room temperature under pressure.

2.3. Characterizations

To unravel the relationship between processing, structure and physical properties, different characterizations were carried out. To master the crosslinking reaction by tuning the materials composition, the gel content of the samples was measured as the ratio of the dry weight of the insoluble fraction and the initial weight. The different materials were characterized morphologically by atomic force microscopy (AFM) and by scanning electron microscopy (SEM). According to the solubility of the samples, different fractions were accurately separated, and their structural analyses were performed by size-exclusion chromatography (SEC) and solid-state nuclear magnetic resonance (ss-NMR) spectroscopy. The crystallinity of the materials was evaluated by X-ray diffraction (XRD). Thermal and mechanical properties were investigated by thermogravimetric analysis (TGA), differential scanning calorimetry (DSC), dynamic mechanical thermal analysis (DMTA) and tensile tests. Rheological behavior was assessed by dynamic shear rheology and creep tests. Details on the characterization methods are reported in the SI (Materials characterization details).

3. Results and discussion

3.1. Reactive melt processing

One-step melt branching/crosslinking initiated by benzoyl peroxide and assisted by water was designed with the aim of improving PCL thermomechanical and rheological properties (Fig. 1). The rationale

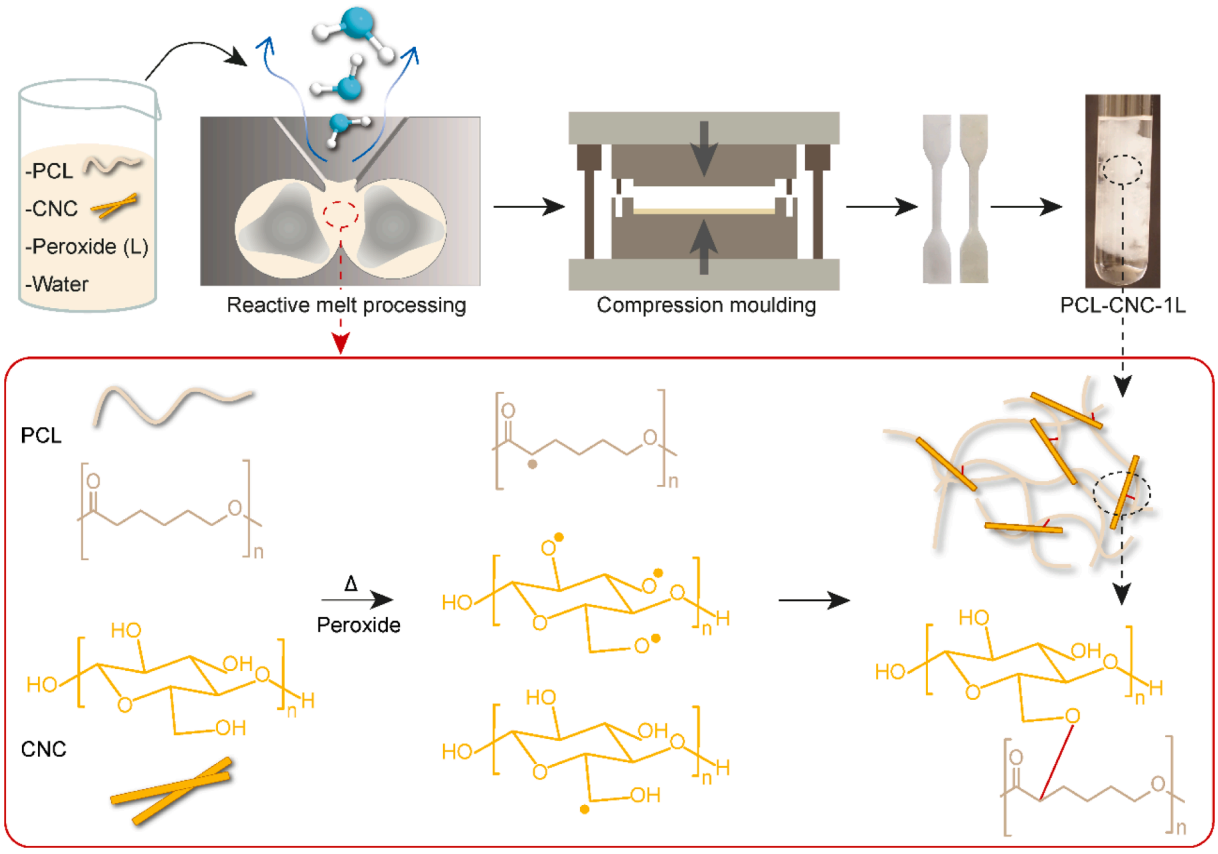

Fig. 1. Top: scheme of reactive melt processing, compression molding, photographs of tensile specimens and dispersions in dichloromethane of the reacted bionanocomposite. Bottom: scheme of reaction with formation of radicals on preferential positions in PCL and CNCs [24] and a possible grafting linkage. (For interpretation of the references to color in this figure legend, the reader is referred to the web version of this article.)

behind this design was to investigate for the first time a possible synergy between the improved CNC dispersion by wet-feeding [19] and the beneficial effect of water in PCL melt radical crosslinking [27]. Bionanocomposites based on CNC (10 wt%) and PCL were successfully produced according to the designed REx in an internal mixer. The synergy and the net contribution of CNC were studied by comparing the bionanocomposites with the PCL reference crosslinked under the same conditions and reagents, including water.

The peroxide content was varied up to 1 wt% to evaluate how different crosslinking degree can affect the bionanocomposites properties, while preserving their processability [27]. It is worth to note that a degree of crosslinking higher than 40 % would hamper the PCL thermoplasticity. Already at 1 wt.% peroxide, a substantial torque increase, *i.e.,* viscosity increase, was registered, confirming the upper limit set in our experiment. For the sake of maximizing the gel content, a reference with 3 wt.% peroxide was anyway prepared, circumventing the high torque by halving the processed mass in the internal mixer. However, due to the thermoset nature of this material, specimens for characterizations could not be molded and only structural analysis could be performed.

3.2. Structural analyses

The effects of CNC and peroxide content on REx were studied by structural analyses. To enable the assessment of gel content and structural analyses according to samples solubility (SEC or ss-NMR), soluble and insoluble fractions were separated first by a 72 h Soxhlet extraction using DCM. Eventually free CNCs (not irreversibly incorporated in the crosslinked network) were precipitated by repeated centrifugation steps (Figure S2). The crosslinking degree was evaluated as the gel content by the ratio between the dry weight of the final extracted insoluble fraction (after centrifugation) and the starting weight of the sample. A gel content of 34 and 38 % was measured for PCL-1L and PCL-CNC-1L, respectively.

The visual appearance of the DCM dispersions shows a transparent gel for PCL-1L and a milky gel for PCL-CNC-1L, the latter reflecting the pale white color of CNC (Fig. 2). The milky appearance given by CNC to PCL-CNC disappears after 24 h due to CNC precipitation (leaving only a transparent PCL solution). The milky appearance of the PCL-CNC-1L gel is instead stable in time, suggesting the irreversible incorporation of CNCs in the gel.

SEC or ss-NMR analyses were carried out to characterize the chemical structure of the different fractions according to their solubility. After centrifugation, only the characteristic signals of CNC were detected in the cross-polarization magic angle spinning (^{13}C CP/MAS) NMR spectrum of the precipitated fraction of PCL-CNC-1L (Fig. 4iv and 3.2.2 Insoluble fractions). This evidence supports the gravimetrical assessment that ≈ 70 wt% of initial CNC amount was permanently incorporated in the insoluble gel.

The insoluble gels of the reacted bionanocomposite and its reference (PCL-CNC-1L and PCL-1L) were observed by optical microscopy after swelling in DCM (Fig. 2). Comparable translucent clusters of dense 3D gel are visible in both materials. However, the micrographs show an increased number of clusters and their size distribution in the gel of the bionanocomposite, suggesting CNCs as crosslinking points. No CNC aggregates could be found at the microscale tested, demonstrating good CNC dispersion.

3.2.1. Soluble fractions

Radical reactions are expected to progress from branching (chain

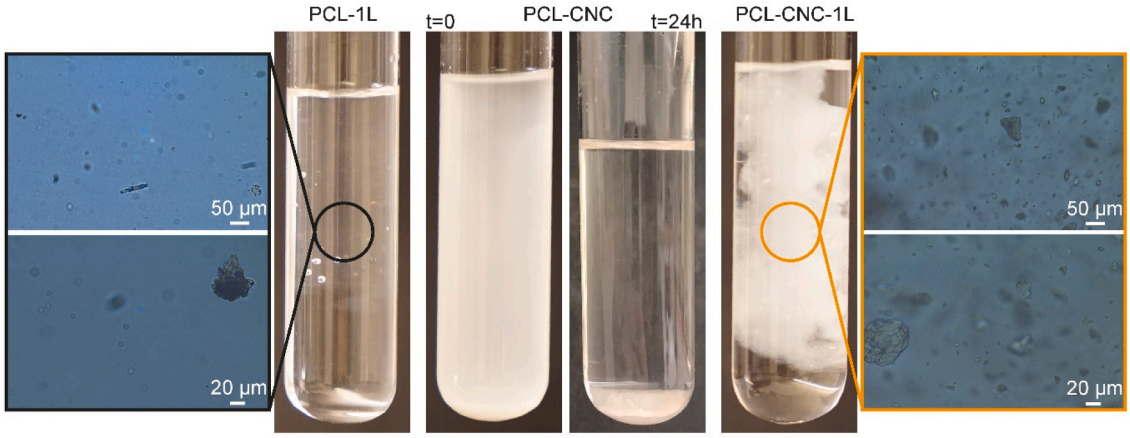

Fig. 2. Dispersions in DCM (0.6 g in 30 mL) after 24 h of PCL-1L and PCL-CNC-1L (left and right images) and optical micrographs of their respective insoluble gels in two different magnifications (scale bars 50 and 20 µm). Dispersion in DCM of PCL-CNC captured at 0 and 24 h after stirring (central images). (For interpretation of the references to color in this figure legend, the reader is referred to the web version of this article.)

extension), thus increasing PCL molecular weight ($\overline{M_w}$) and polydispersity, towards crosslinked 3D insoluble networks.

SEC was used to analyze PCL molecular structure changes in the soluble fractions to assess the progress of the reaction varying the composition and the peroxide content. However, SEC analysis does not include nanogels eventually escaping the Soxhlet thimble, which would be blocked by the filter for SEC sample preparation. Therefore, this population is neither represented in the SEC nor in the insoluble fractions' analyses.

The PCL reacted with 0.5 wt% of peroxide (sPCL-0.5L) shows almost doubled $\overline{M_w}$ and polydispersity, compared to neat PCL (Fig. 3). This result confirms the efficiency of the reaction and suggests the branching of PCL below its gelation. A further increased branching is observed in the SEC analysis of sPCL-1L, with a 150 % increase of $\overline{M_w}$ and tripled polydispersity compared to neat PCL (obviously even high molecular weight is expected in its 34 % insoluble gel). At higher peroxide content (3 wt%), as the majority of PCL is crosslinked (74 % gel content), $\overline{M_w}$ of the soluble fraction substantially decreases. These lower molecular weight chains can result from both β-scission induced by higher amount of peroxide and promotion of branched macromolecules to the 3D crosslinked insoluble network [36]. Structural analysis confirms that branching progresses towards crosslinking with increasing peroxide content. At 1 wt.% peroxide the bionanocomposite shows higher molecular weight (above 30 % increase of $\overline{M_w}$) and lower polydispersity compared to its reference, confirming that CNCs contribute to the radical reaction and suggesting grafting onto CNCs of lower M_w PCL. The lower molecular weight PCL chains, more hydrophilic and keener to migrate at the PCL/CNC interface, can justify the better CNC dispersion observed in the crosslinked bionanocomposite (Fig. 2).

3.2.2. *Insoluble fractions*

The neat PCL and CNC, and insoluble fractions at 1 wt.% peroxide (gels and precipitate from Soxhlet extraction and centrifugation) were studied by solid-state NMR spectroscopy. Using assignments from the literature, ^{13}C NMR signals for PCL [37] and CNC [38] were identified and summarized (Fig. 4).

The five spectra clearly show signals of PCL (Fig. 4i-iii) and CNC (Fig. 4iii-v). Assuming that crosslinking would occur according to the literature [36], between C2-carbons (α-carbons) of PCL (Fig. 1), one would expect a new C2-carbon signal predicted to arise around 45 ppm [39] in the spectrum of the gel fraction of PCL-1L. For the sake of deeper understanding, we have further investigated the structure of this radical reaction on a model system, which led us to similar conclusions (Mechanism of PCL radical reaction in SI). However, no signal around 45 ppm could be distinguished in the spectrum. The spectra of neat PCL (Fig. 4i) and that of the gel fraction of PCL-1L (Fig. 4ii) are too similar to draw any conclusion about possible molecular modifications. Similarly, there are no detectable signals indicating any new covalent bonds in the

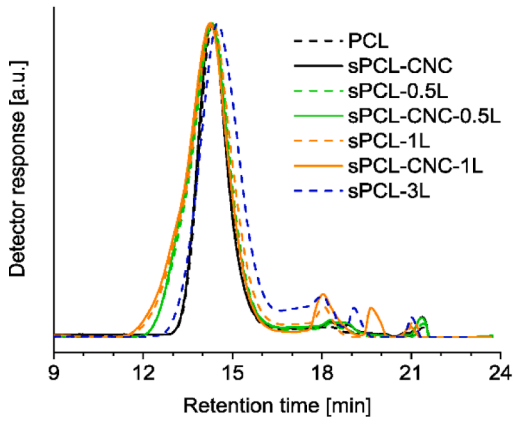

Material	$\overline{M_n}$ [g·mol^{-1}]	$\overline{M_w}$ [g·mol^{-1}]	Đ
PCL	77,000	150,000	2
sPCL-CNC	80,000	160,000	1.96
sPCL-0.5L	86,000	290,000	3.37
sPCL-CNC-0.5L	91,000	300,000	3.38
sPCL-1L	63,000	374,000	5.92
sPCL-CNC-1L	95,000	477,000	5
sPCL-3L	41,000	125,000	3.06

Fig. 3. SEC chromatographs of soluble fractions (linear and branched chains) in chloroform and table summarizing their number ($\overline{M_n}$) and weight ($\overline{M_w}$) average molecular weights, and polydispersity (Đ). "s" prefix indicates that the analysis reflects only the soluble fraction of the samples. (For interpretation of the references to color in this figure legend, the reader is referred to the web version of this article.)

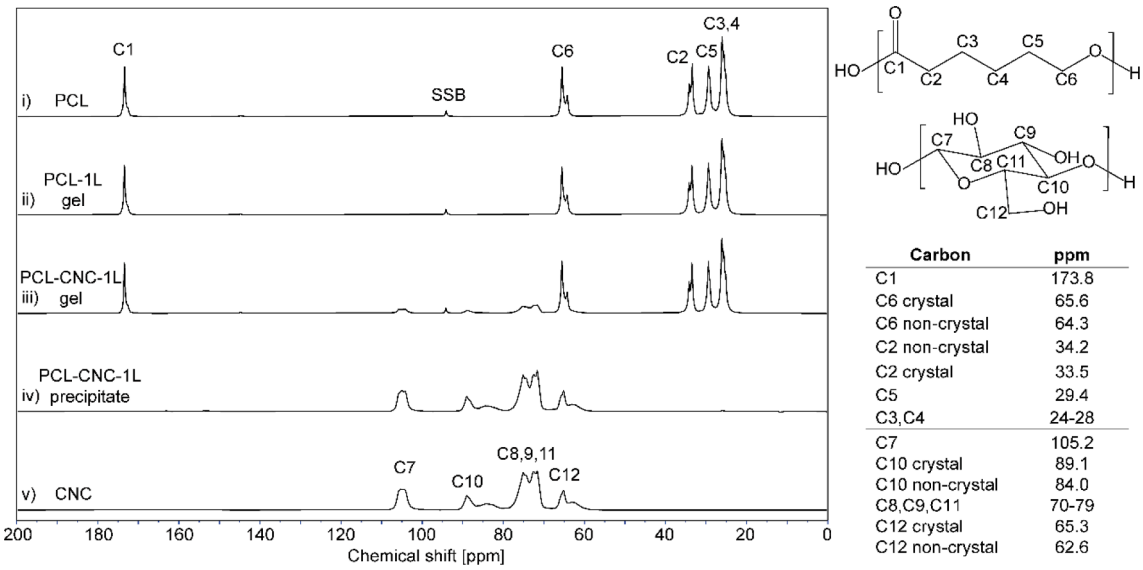

Carbon	ppm
C1	173.8
C6 crystal	65.6
C6 non-crystal	64.3
C2 non-crystal	34.2
C2 crystal	33.5
C5	29.4
C3,C4	24-28
C7	105.2
C10 crystal	89.1
C10 non-crystal	84.0
C8,C9,C11	70-79
C12 crystal	65.3
C12 non-crystal	62.6

Fig. 4. The ^{13}C CP/MAS NMR spectra of (i) neat PCL, gels of (ii) PCL-1L and (iii) PCL-CNC-1L, (iv) precipitate of PCL-CNC-1L, (v) neat CNC. SSB denotes spinning side band. In spectrum (iii) of gel fraction of PCL-CNC-1L, characteristic peaks of both neat CNC (v) and PCL (i) are clearly visible, indicating the irreversible incorporation of CNC in the gel. Inset on the bottom right side shows molecular structures of (upper) PCL and (lower) CNC as well as a table specifying their ^{13}C chemical shifts. (For interpretation of the references to color in this figure legend, the reader is referred to the web version of this article.)

spectra of gel fraction of PCL-CNC-1L (Fig. 4iii).

Since the expected signal after successful crosslinking should be well resolved from all other signals, the noise level for the experiments could be used to estimate the level-of-detection (LOD) for such a signal (method in SI) [40]. The obtained LOD was compared to the C6 signal of PCL at 64.3 ppm normalized to 100 %. If covalent crosslinking has taken place, the degree of crosslinks per repeating unit of the polymer would be less than 2.5 %, as calculated from the spectral signal-to-noise (Fig. 4ii, Equation S4 and details in SI). Using a PCL $\overline{M}_w$ of 100,000 g·mol^{-1}, as provided by the supplier, corresponding to approximately 880 repeating units, this threshold would correspond to at least 22 crosslinks per polymer chain. In other words, crosslinking can only be registered in the NMR spectra above the threshold of 22 crosslinks per chain, which would correspond to a thermoset polymer with 100 % gel content. The lack of a visible signal from a crosslinked C2 should hence not be seen as a sign of failed crosslinking but rather an outcome of limited analysis method.

From ^{13}C CP/MAS NMR spectra, CNC and PCL signals are clearly detected in the gel fraction of PCL-CNC-1L (Fig. 4iii) and only CNC in its precipitate (Fig. 4iv). Although the presence of CNCs in the gel fraction could theoretically be due also to physically trapped CNCs in inextricable PCL networks, the thorough Soxhlet extraction and subsequent centrifugation ensures that unreacted CNCs are separated from the floating gel fraction. As no PCL signal was observed in the latter, the precipitate is composed only by CNC, which by gravimetrical assessment corresponds to 30 wt% of the initial CNC amount. Therefore, we can conclude that the 70 wt% of the CNCs was irreversibly incorporated in the gel. Due to the higher density of CNC compared to the DCM solvent, one would expect all CNCs to end up in the precipitate in the absence of significant polymer grafting onto CNCs. Moreover, the random proton extraction by the peroxide leads to the formation of CNC radicals (Fig. 1) [24] which would react with the more mobile macromolecules, such as shorter PCL chains. These are strong indications, albeit indirect, that our water-assisted REx design successfully crosslinks PCL and CNCs. These results indicate the formation of a network in which CNCs are rigid crosslinking junctions, leading to a unique structurally different gel compared to the one in PCL-1L.

3.3. Melt rheology

Dynamic rheology (at 120 °C) was carried out to puzzle out how the branching/crosslinking and the different network structure (with or without CNC) affect the materials melt behavior.

From the frequency sweep curves, PCL and PCL-CNC are characterized by a liquid-like melt as the loss moduli are greater than the storage ones over the entire frequency range (Fig. 5a). The addition of CNC does not affect the PCL rheological behavior, because of the observed poor adhesion and CNC aggregation, despite the high CNC content selected. These results confirm that traditional melt processing does not lead to a CNC percolating network, as previously observed [32]. By water-assisted REx design, an increase of gel content enhances PCL viscosity and moduli up to two and four orders of magnitude, respectively (Fig. 5a and 5b). These unprecedented results point at a uniform branching/crosslinking achieved via our REx design. For the bionanocomposite with 0.5 wt.% peroxide a crossover between loss and storage moduli ($G' = G''$) is reached at lower frequency compared its reference (≈ 5 rad·s^{-1} and ≈ 70 rad·s^{-1} for PCL-CNC-0.5L and PCL-0.5L, respectively), signifying a shift from viscous to solid-like behavior. At 1 wt.% peroxide the storage moduli become prevalent over the entire frequency range. Both results point to a slower relaxation (longer relaxation time) in the reacted bionanocomposites, compared to the mere effect of higher $\overline{M}_w$ of the branched/crosslinked matrix. This is consistent with the different bionanocomposite network demonstrated in the structural analyses and highlights the contribution of the rigid CNC junctions on PCL rheological properties.

The change from viscous to elastic character is also proven by the Van Gurp-Palmen plot (Fig. 5c), which displays the phase angles as a function of the absolute value of the complex shear modulus. A predominant melt elasticity is indicated by low phase angles (below 45°) [41]. The materials reacted with 1 wt.% peroxide show phase angles below 40°, while the unreacted PCL and PCL-CNC maintain phase angles $\approx$ 90°, typical of a viscous behavior. Increasing the peroxide content progressively lowers the phase angles, further reduced by CNC, acting as rigid elastic junctions in the network.

Complex viscosities show that the linear Newtonian behavior of PCL and PCL-CNC changes to shear thinning for all the frequency range more and more pronounced with the increase of branching/crosslinking (Fig. 5b). Relatively low viscosities at high frequencies are maintained,

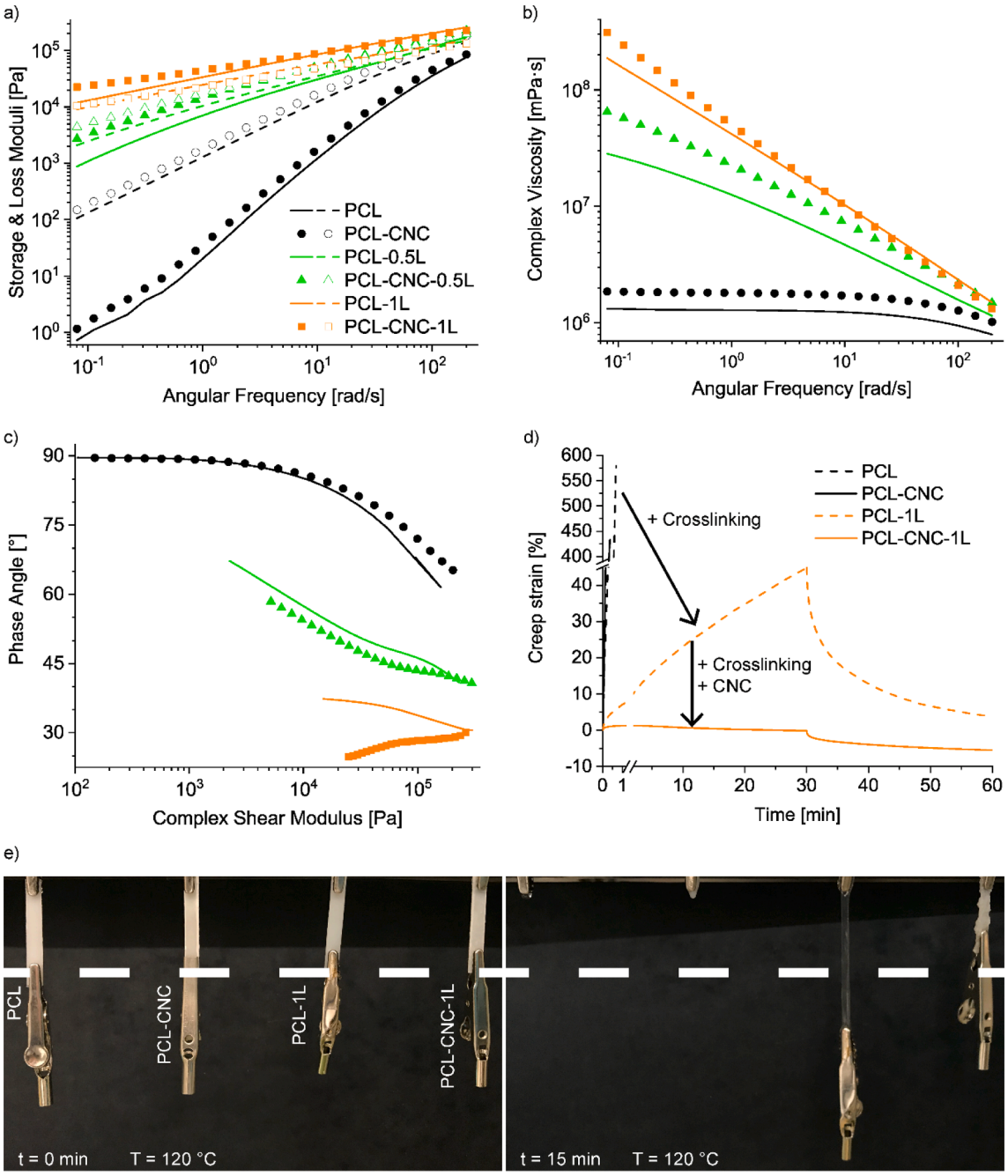

Fig. 5. Dynamic rheological frequency sweeps at 120 °C: (a) storage (full symbols and solid lines) and loss (empty symbols and dashed lines) moduli; (b) complex viscosity; (c) Van Gurp-Palmen plot showing phase angles as a function of complex shear modulus (|G*|). (d) Creep tests at 120 °C of the unreacted and reacted bionanocomposites and respective references. (e) Visualization of heat-shrinking by loading unreacted and reacted bionanocomposites and respective references with a weight of ≈ 3.5 g (≈ 7 kPa) in an oven at 120 °C, at 0 and 15 min. (For interpretation of the references to color in this figure legend, the reader is referred to the web version of this article.)

predicting a further decrease in viscosity at the even higher shear rates. On one hand REx increased PCL melt elasticity, correlated to higher melt strength [25]. On the other our REx preserves PCL processability, since typical melt processing techniques require higher shear rates ($>10^2\ s^{-1}$). Further studies on the processability and the transfer of this approach to continuous melt processing are in progress.

For comparison, Wei et al. [25] obtained an increase of moduli of three orders of magnitude by reacting PHB with DCP at 20 wt% cellulose fibers. Nanthananon et al. [42] have achieved a similar increase to our results in bionanocomposites' moduli and viscosity by the use of di(*tert*-butylperoxyisopropyl)benzene for melt crosslinking PLA with 10 wt% cellulose fibers. Focusing on nanocelluloses, Li et al. [23] have achieved two and three orders of magnitude in the relative increase of PLA viscosity and moduli in 5 wt% cellulose nanofibrils biocomposites crosslinked with DCP. However, the latter cited references lack clear proof of grafting onto PLA, and the recorded improvement cannot be selectively assigned to the cellulose as the references of crosslinked matrix are not considered. Moreover, both used celluloses have greater aspect ratio than our CelluForce CNCs.

3.4. Melt creep

The improved dimensional stability of bionanocomposites is of interest for applications in which low melting biopolymers, such as PCL, are likely to fail. Creep tests at 120 °C were carried out on the higher gel content materials (PCL-1L and PCL-CNC-1L) and compared to the references to study the effect of the 3D network. The mere addition of CNC does not influence PCL creep behavior, rapidly reaching high strain and failure in ≈ 30 s (Fig. 5d), due to the poor melt strength of PCL and easy chains alignment in the melt (liquid-like behavior). Crosslinked PCL maintains creep below 50 %, with almost complete recovery, consistent with hindered chain mobility and corroborating the homogeneity of the PCL network distribution, as previously observed for radiation crosslinked PCL [43]. The addition of CNC in REx, instead, lead to a unique behavior where shrinkage combines with creep: first the material creeps with only minor deformation, then it uniformly shrinks up to negative strain values. This homogeneous shrinkage, also defined as heat-shrinking, can be achieved only through a synergy between CNC dispersion and CNC participation in a 3D co-continuous network. The co-continuity of the network and its uniform distribution in the melt promote a reversible recovery, relevant for shape-memory ability. Shrinkage upon heating is a typical behavior of rubbers [29,44], indicating the elastomeric character of the thermoplastic/thermoset bionanocomposite obtained by our controlled REx. When the bionanocomposite is compression molded at 120 °C, the cooling under pressure "freezes" the covalently bonded chains in a stretched uncoiled state at low entropy. When exposing again the sample to a temperature above melting under a uniaxial load, the chains return quickly to their high entropy relaxed state in which the CNC rigid elastic junctions serve as memory points, enabling heat-shrinking (entropy-driven shape recovery) [45]. The superior elasticity of the PCL-CNC-1L network reflects the contribution of CNCs effectively dispersed towards the exploitation of their potential "nano-effect".

The heat-shrink feature was visually evaluated by exposing materials bars to the same temperature of the creep tests (120 °C) under a constant load of ≈ 7 kPa (clamps of ≈ 3.5 g) (Fig. 5e). After less than 1 min the unreacted samples broke, while after 15 min PCL-1L elongated and PCL-CNC-1L shrank. The resistance to deformation and heat-shrinkage under small loads have been reported for radiation crosslinked PCL but only at gel content above 80 %, *i.e.,* when PCL cannot be melt processed [43].

3.5. Thermomechanical properties

TGA was carried out to investigate the influences of REx and possible cellulose degradation during processing on the thermal stability of the materials. The thermograms of all the bionanocomposites (Figure S5) show two major degradation peaks which reflect the degradation of CNC and PCL, respectively. CNC degradation step is shifted to higher temperatures (from 276 to 291 °C for PCL-CNC and PCL-CNC-1L, respectively) in line with the incorporation of CNCs in the network by grafting of PCL onto CNC and homogeneous CNC dispersion which delays degradation (Figure S5; Table S2) [22,24,25].

Thermal transitions changes induced by REx were examined by DSC. By increasing peroxide content, the crystallization temperature (from cooling scans) increases, together with a crystallization broadening (Figure S6; Table S2). These changes are consistent with a nucleating effect played by branching/crosslinking points [46], facilitating the crystallization at higher temperature. Higher polydispersity, leading to more heterogenous crystal structures, explains the observed crystallization broadening [47]. CNCs delay the crystallization, as previously reported for similar CNC content bionanocomposites [48]. However, this delay decreases with crosslinking, in line with improved CNCs dispersion suggested in the gel microscopy (Fig. 2).

Crystalline fractions and crystallite sizes have been further evaluated by XRD (Figure S7; Table S3). The diffraction spectra of all the tested materials show two main crystalline peaks (32.1° and 35.6°), related to (1 1 0) and (2 0 0) PCL crystallographic lattices [49]. Crosslinking leads to an increase of crystallinity and crystal lattice size, as observed in crosslinked PLA [22,23]. In PCL-CNC-1L, the rigid elastic junctions provided by CNCs to the 3D network result in greater crystallinity compared to PCL-1L. To further elucidate on the mechanisms of crystallinity changes, the different crystallites volumes and the number of crystallites per μm^3 were calculated (Table S3). Crosslinking greatly enlarges the crystallites, because of hindered chain folding, but reduces the crystallites number in a volume unit. Cross-referencing DSC and XRD results (Figure S6b, Table S2, Figure S7, and Table S3) we can conclude that crosslinking leads to a faster crystal growth, which can be ascribed to the lower molecular weight PCL chains formed by β-scission (Fig. 3). CNCs initiate a larger number but smaller crystallites, confirming their nucleating effect. While in PCL-CNC the increased number of nuclei is prevalent to their growth, thus lowering the overall crystallinity, in the crosslinked bionanocomposite the faster crystallite growth further contributes to the highest crystallinity. In highly crosslinked (over 60 %) polymers, it has been reported that the crosslink junctions disturb the reorganization and chain folding, leading to a decrease in crystallinity and spherulite size [7,50]. Instead, in our system where the 60 % of PCL chains with higher polydispersity are still free to move, we have registered an increase in crystallinity at the ≈ 40 % of gel content.

The DMTA temperature sweep were carried out as a more sensitive analysis than DSC for capturing the thermal transitions. The detected PCL glass (T_g) and alpha transitions shift towards higher temperatures when branching/crosslinking occurred in the presence of CNC pointing at restricted PCL chain mobility (Figure S8; Table S4). The mere addition of CNCs leads to a decrease in storage modulus below T_g due to poor CNC dispersion and interaction with the PCL, while above T_g CNCs stiffen PCL according to the lower damping factor. The PCL branching leads initially to a decrease in the storage modulus due to the plasticizing effect of shorter PCL chains (PCL-0,5L), followed by a stiffening when the crosslinking becomes predominant (PCL-1L). Only when CNCs and crosslinking are combined, the storage modulus increases over the entire temperature range. This result indicates crosslinking and CNCs synergy and is consistent with a reduced PCL chain mobility (higher T_g).

The mechanical behavior of the materials has also been assessed by tensile tests to evaluate the effect of REx on PCL deformability and toughness. The unreacted bionanocomposite shows the detrimental effect of CNCs on PCL tensile properties, as previously reported for extruded PCL-CNC at the same ratio [32]. Increasing the crosslinking degree (PCL-CNC-1L) reduces the deformability, consistent with shorter chain lengths between crosslinks (Fig. 6a and S9; Table S5) [51]. After yielding, this bionanocomposite directly undergoes a pronounced strain hardening, further pointing to a co-continuous network below melting ($T_g < RT < T_m$). The large number of evenly distributed crosslinking points enables an effective stretching and orientation of the interconnected molecular chains, hence hindering disentanglements typical of the PCL rubbery plateau, as schematized in Fig. 6b. Moreover, the proven incorporation of CNCs in the gel strengthens the network, providing more efficient stress transfer.

The SEM micrographs show different tensile fracture modes in PCL-CNC (Fig. 6c) and PCL-CNC-1L (Fig. 6d) at room temperature. The unreacted bionanocomposite shows a highly ductile surface fracture characterized by elongated polymer fibrils, typical of PCL fractured largely above its glass transition [52]. Crack propagation locally increases temperature, thus leading to PCL deformation (fibrillation) and finally to failure. In PCL-CNC, large CNC agglomerates are visible among the PCL fibrils, indicating poor dispersion. The fracture surface of the crosslinked bionanocomposite instead is relatively smooth, with reduced fibrillation. Fewer and smaller agglomerates are present and seem more embedded in the matrix, suggesting a higher dispersion. In support, the micrographs obtained by transmission electron microscopy of cryo-microtomized samples (Figure S10) show no aggregates in the crosslinked bionanocomposite, while CNC clusters are visible in the unreacted one. Both morphological analyses are consistent with a

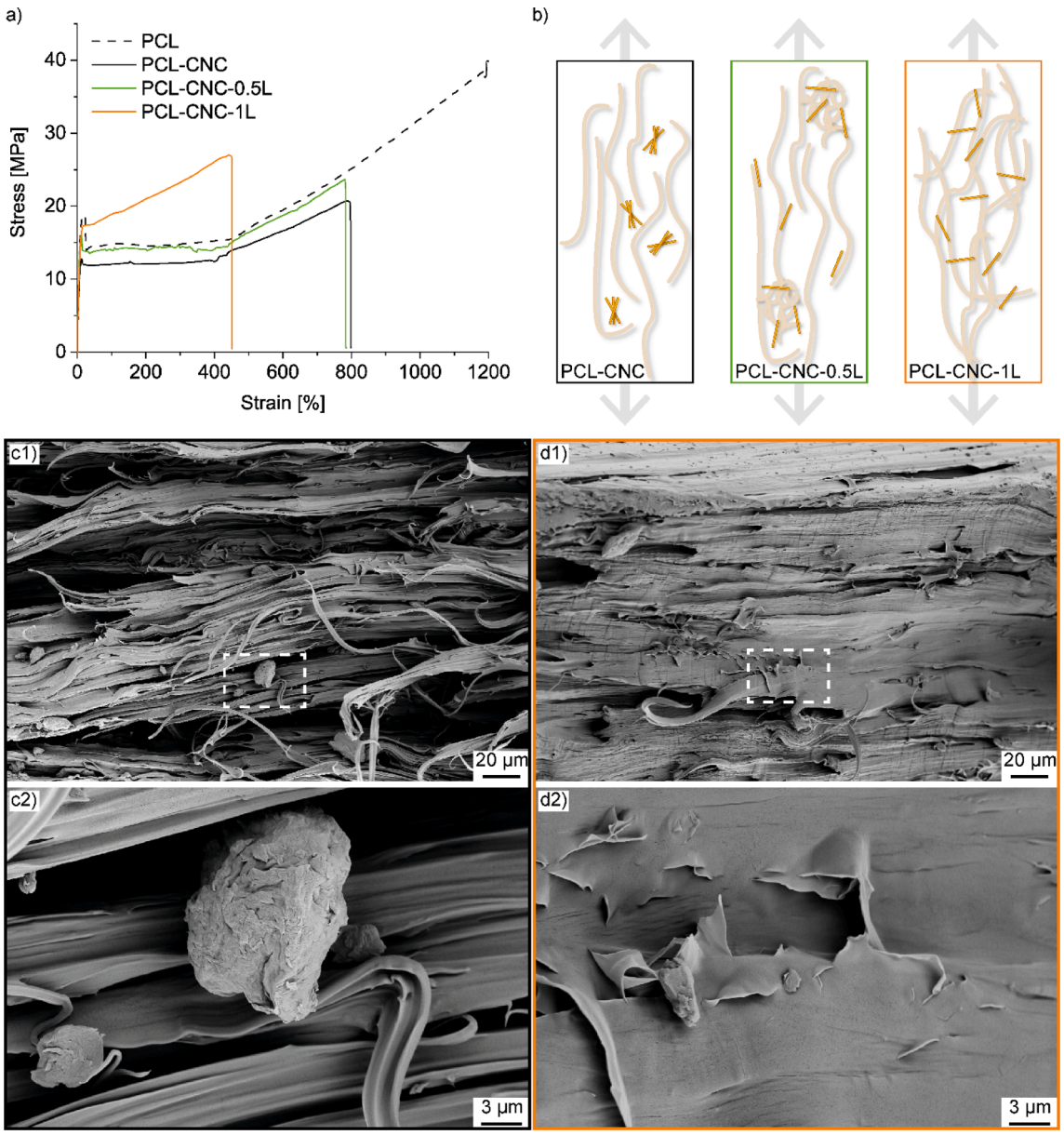

Fig. 6. (a) Representative tensile curves of unreacted and reacted bionanocomposites with (b) schemes of their nanostructure under tensile load. SEM micrographs of tensile fractured surfaces of (c1) PCL-CNC and (d1) PCL-CNC-1L (scale bars 20 µm) and their magnification (c2) and (d2), respectively (scale bars 3 µm). (For interpretation of the references to color in this figure legend, the reader is referred to the web version of this article.)

chemical grafting of PCL onto CNC surface.

4. Conclusions

We have designed a green water-assisted strategy to prepare thermoplastic/thermoset PCL/CNC bionanocomposites via one-step reactive melt processing. Water served a bifunctional role: 1) suspension medium for wet-feeding individualized CNCs and 2) booster of radical reactions. The results demonstrated that water leads to a synergic effect between CNC dispersion and crosslinking. Structural analyses indicate that the designed REx led to bionanocomposites with gel content up to ≈ 40 %, which irreversibly incorporates the majority of CNCs. The dynamic melt rheology showed that the higher the gel content, the higher the elastic character, which further improved with CNCs participation to the network. In the reacted bionanocomposite, the increase in complex viscosity and an enhanced shear thinning behavior corroborated a reduced molecular mobility due to the rigid elastic CNC junctions. The superior melt creep resistance indicated the percolation of the crosslink junctions in the network. The crosslinked bionanocomposite exhibited unprecedented entropy-driven heat-shrinkage at 40 % gel content, confirming the co-continuity of the network and the CNC/crosslinking synergy achieved by our water-assisted REx.

Our work highlights the possibility to use CNCs in controlled reactive melt processing for thermoplastic/thermoset bionanocomposites with improved rheological performance. The mere resistance to creep suggests the REx bionanocomposites as a possible replacement for non-biodegradable extruded profiles and packaging, for which high melt strength and shape retention at high temperatures are crucial. The disclosed heat-shrinkage has potential for new sustainable materials for shape-memory applications and tests are in progress to deeper evaluate the shape-recovery. The obtained results motivate the crucial verification of recyclability and biodegradability of the bionanocomposites to validate their sustainable end-of-life options.

CRediT authorship contribution statement

Angelica Avella: Conceptualization, Investigation, Writing – original draft, Visualization. **Alexander Idström:** Investigation, Writing – original draft. **Rosica Mincheva:** Conceptualization, Investigation, Writing – review & editing, Supervision, Validation. **Koyuru Nakayama:** Investigation, Writing – original draft. **Lars Evenäs:** Writing – review & editing, Supervision, Validation. **Jean-Marie Raquez:** Writing – review & editing, Supervision. **Giada Lo Re:** Conceptualization, Writing – review & editing, Funding acquisition, Supervision, Validation.

Declaration of Competing Interest

The authors declare that they have no known competing financial interests or personal relationships that could have appeared to influence the work reported in this paper.

Data availability

Data will be made available on request.

Acknowledgements

Giada Lo Re acknowledges Knut and Alice Wallenberg Biocomposites [grant number V-2019-0041, Dnr. KAW 2018.0551] and Chalmers Genie for financial support. Dr. Abhijit Venkatesh is gratefully acknowledged for the AFM analysis. The solid-state NMR measurements were conducted at the NMR Core Facility at Umeå University, Sweden, with the assistance of Dr. Tobias Sparrman. We thank Lisa Dangreau and Yoann Paint, MateriaNova, Mons, Belgium, for their help with the microscopy.

Appendix A. Supplementary data

Supplementary data to this article can be found online at https://doi.org/10.1016/j.compositesa.2022.107166.

References

[1] Geyer R, Jambeck JR, Law KL. Production, use, and fate of all plastics ever made. Sci Adv 2017;3:e1700782. https://doi.org/10.1126/sciadv.1700782.
[2] European Bioplastics. Bioplastics market data 2022. https://www.european-bioplastics.org/market/ (accessed February 21, 2022).
[3] Raquez JM, Narayan R, Dubois P. Recent advances in reactive extrusion processing of biodegradable polymer-based compositions. Macromol Mater Eng 2008;293:447–70. https://doi.org/10.1002/mame.200700395.
[4] United Nations. THE 17 GOALS | Sustainable Development 2022. https://sdgs.un.org/goals (accessed February 21, 2022).
[5] Kaldéus T, Träger A, Berglund LA, Malmström E, Lo Re G. Molecular engineering of the cellulose-poly(caprolactone) bio-nanocomposite interface by reactive amphiphilic copolymer nanoparticles. ACS Nano 2019;13:6409–20. https://doi.org/10.1021/acsnano.8b08257.
[6] Kotcharat P, Chuysinuan P, Thanyacharoen T, Techasakul S, Ummartyotin S. Development of bacterial cellulose and polycaprolactone (PCL) based composite for medical material. Sustain Chem Pharm 2021;20:100404. https://doi.org/10.1016/j.scp.2021.100404.
[7] Han C, Ran X, Su X, Zhang K, Liu N. Effect of peroxide crosslinking on thermal and mechanical properties of poly (ε -caprolactone). Polym Int 2007;600:593–600. Doi: 10.1002/pi.
[8] Przybysz M, Hejna A, Haponiuk J, Formela K. Structural and thermo-mechanical properties of poly(ε-caprolactone) modified by various peroxide initiators. Polymers 2019;11:1101. https://doi.org/10.3390/polym11071101.
[9] Gandhi K, Kriz D, Salovey R, Narkis M, Wallerstein R. Crosslinking of polycaprolactone in the pre-gelation region. Polym Eng Sci 1988;28:1484–90. https://doi.org/10.1002/pen.760282209.
[10] Di Maio E, Iannace S, Marrazzo C, Narkis M, Nicolais L. Effect of molecular modification on PCL foam formation and morphology of PCL. Macromol Symp 2005;228:219–28. https://doi.org/10.1002/masy.200551019.
[11] Yoshii F, Darwis D, Mitomo H, Makuuchi K. Crosslinking of poly(ε-caprolactone) by radiation technique and its biodegradability. Radiat Phys Chem 2000;57:417–20. https://doi.org/10.1016/S0969-806X(99)00449-1.
[12] Li T, Chen C, Brozena AH, Zhu JY, Xu L, Driemeier C, et al. Developing fibrillated cellulose as a sustainable technological material. Nature 2021;590(7844):47–56.
[13] Fujisawa S, Saito T, Kimura S, Iwata T, Isogai A. Surface engineering of ultrafine cellulose nanofibrils toward polymer nanocomposite materials. Biomacromolecules 2013;14:1541–6. https://doi.org/10.1021/bm400178m.
[14] Sakakibara K, Moriki Y, Yano H, Tsujii Y. Strategy for the Improvement of the Mechanical Properties of Cellulose Nanofiber-Reinforced High-Density Polyethylene Nanocomposites Using Diblock Copolymer Dispersants. ACS Appl Mater Interfaces 2017;9:44079–87. https://doi.org/10.1021/acsami.7b13963.
[15] Gindl-Altmutter W, Obersriebnig M, Veigel S, Liebner F. Compatibility between Cellulose and Hydrophobic Polymer Provided by Microfibrillated Lignocellulose. ChemSusChem 2015;8:87–91. https://doi.org/10.1002/cssc.201402742.
[16] Zheng T, Pilla S. Melt Processing of Cellulose Nanocrystal-Filled Composites: Toward Reinforcement and Foam Nucleation. Ind Eng Chem Res 2020;59:8511–31. https://doi.org/10.1021/acs.iecr.0c00170.
[17] Clemons C, Sabo R. A Review of Wet Compounding of Cellulose Nanocomposites. Polymers 2021;13(6):911.
[18] Lo Re G, Engström J, Wu Q, Malmström E, Gedde UW, Olsson RT, et al. Improved Cellulose Nanofibril Dispersion in Melt-Processed Polycaprolactone Nanocomposites by a Latex-Mediated Interphase and Wet Feeding as LDPE Alternative. ACS Appl Nano Mater 2018;1(6):2669–77.
[19] Lo Re G, Sessini V. Wet feeding approach for cellulosic materials/PCL Biocomposites. In: ACS Symp Ser Am Chem Soc. 1304. Washington, DC: American Chemical Society; 2018. p. 209–26. https://doi.org/10.1021/bk-2018-1304.ch011.
[20] Lo Re G, Spinella S, Boujemaoui A, Vilaseca F, Larsson PT, Adås F, et al. Poly(ε-caprolactone) Biocomposites Based on Acetylated Cellulose Fibers and Wet Compounding for Improved Mechanical Performance. ACS Sustain Chem Eng 2018;6(5):6753–60.
[21] Imre B, García L, Puglia D, Vilaplana F. Reactive compatibilization of plant polysaccharides and biobased polymers: Review on current strategies, expectations and reality. Carbohydr Polym 2019;209:20–37. https://doi.org/10.1016/j.carbpol.2018.12.082.
[22] Dhar P, Tarafder D, Kumar A, Katiyar V. Thermally recyclable polylactic acid/cellulose nanocrystal films through reactive extrusion process. Polymer (Guildf) 2016;87:268–82. https://doi.org/10.1016/j.polymer.2016.02.004.
[23] Li FJ, Yu XT, Huang Z, Liu DF. Interfacial improvements in cellulose nanofibers reinforced polylactide bionanocomposites prepared by in situ reactive extrusion. Polym Adv Technol 2021;32:2352–66. https://doi.org/10.1002/pat.5264.
[24] Wei L, McDonald AG, Stark NM. Grafting of Bacterial Polyhydroxybutyrate (PHB) onto Cellulose via In Situ Reactive Extrusion with Dicumyl Peroxide. Biomacromolecules 2015;16:1040–9. https://doi.org/10.1021/acs.biomac.5b00049.
[25] Wei L, Stark NM, McDonald AG. Interfacial improvements in biocomposites based on poly(3-hydroxybutyrate) and poly(3-hydroxybutyrate-co-3-hydroxyvalerate) bioplastics reinforced and grafted with α-cellulose fibers. Green Chem 2015;17:4800–14. https://doi.org/10.1039/c5gc01568e.
[26] Zheng T, Clemons CM, Pilla S. Comparative Study of Direct Compounding, Coupling Agent-Aided and Initiator-Aided Reactive Extrusion to Prepare Cellulose Nanocrystal/PHBV (CNC/PHBV) Nanocomposite. ACS Sustain Chem Eng 2020;8:814–22. https://doi.org/10.1021/acssuschemeng.9b04867.
[27] Avella A, Mincheva R, Raquez J-M, Lo RG. Substantial Effect of Water on Radical Melt Crosslinking and Rheological Properties of Poly(ε-Caprolactone). Polymers 2021;13:491–505. https://doi.org/10.3390/polym13040491.
[28] Hong CK, Maeng H, Song K, Kaang S. Thermal behaviors of heat shrinkable poly(vinyl chloride) film. J Appl Polym Sci 2009;112:886–95. https://doi.org/10.1002/APP.29550.
[29] Liu C, Qin H, Mather PT. Review of progress in shape-memory polymers. J Mater Chem 2007;17:1543–58. https://doi.org/10.1039/b615954k.
[30] Venkatesh A, Thunberg J, Sahlin-Sjövold K, Rigdahl M, Boldizar A, Abhijit V, et al. Melt Processing of Ethylene-Acrylic Acid Copolymer Composites Reinforced with Nanocellulose. Polym Eng Sci 2020;60:956–67. https://doi.org/10.1002/pen.25351.
[31] Bourassa P, Methot M, Berry R. Preparation of solvent and polymer redispersible formulations of dried cellulose nanocrystals (cnc). US 2020/0087464 A1, 2020.
[32] Venkatesh A, Forsgren L, Avella A, Banke K, Wahlberg J, Vilaseca F, et al. Water-assisted melt processing of cellulose biocomposites with poly(ε-caprolactone) or poly(ethylene-acrylic acid) for the production of carton screw caps. J Appl Polym Sci 2022;139(6):51615. https://doi.org/10.1002/APP.51615.
[33] Germiniani LGL, da Silva LCE, Plivelic TS, Gonçalves MC. Poly(ε-caprolactone)/cellulose nanocrystal nanocomposite mechanical reinforcement and morphology: the role of nanocrystal pre-dispersion. J Mater Sci 2019;54:414–26. https://doi.org/10.1007/s10853-018-2860-9.
[34] Shen Y, Zhu W, Papadaki M, Mannan MS, Mashuga CV, Cheng Z. Thermal decomposition of solid benzoyl peroxide using Advanced Reactive System Screening Tool: Effect of concentration, confinement and selected acids and bases. J Loss Prev Process Ind 2019;60:28–34. https://doi.org/10.1016/j.jlp.2019.04.001.
[35] Cicogna F, Coiai S, Rizzarelli P, Carroccio S, Gambarotti C, Domenichelli I, et al. Functionalization of aliphatic polyesters by nitroxide radical coupling. Polym Chem 2014;5(19):5656. https://doi.org/10.1039/c4py00641k.
[36] Kim CH, Cho KY, Park JK. Grafting of glycidyl methacrylate onto polycaprolactone: Preparation and characterization. Polymer (Guildf) 2001;42:5135–42. https://doi.org/10.1016/S0032-3861(01)00013-1.
[37] Schäler K, Achilles A, Bärenwald R, Hackel C, Saalwächter K. Dynamics in crystallites of poly(ε-caprolactone) as investigated by solid-state NMR. Macromolecules 2013;46:7818–25. https://doi.org/10.1021/ma401532v.

[38] Kono H, Yunoki S, Shikano T, Fujiwara M, Erata T, Takai M. CP/MAS 13C NMR study of cellulose and cellulose derivatives. 1. Complete assignment of the CP/MAS 13C NMR spectrum of the native cellulose. J Am Chem Soc 2002;124:7506–11. https://doi.org/10.1021/ja010704o.
[39] Bremser W. Hose - a novel substructure code. Anal Chim Acta 1978;103:355–65. https://doi.org/10.1016/S0003-2670(01)83100-7.
[40] Currie LA. Nomenclature in evaluation of analytical methods including detection and quantification capabilities. Pure Appl Chem 1995;67:1699–723. https://doi.org/10.1351/pac199567101699.
[41] Trinkle S, Freidrich C. Van Gurp-Palmen-plot: A way to characterize polydispersity of linear polymers. Rheol Acta 2001;40:322–8. https://doi.org/10.1007/s003970000137.
[42] Nanthananon P, Seadan M, Pivsa-Art S, Hiroyuki H, Suttiruengwong S. Biodegradable polyesters reinforced with eucalyptus fiber: Effect of reactive agents. AIP Conf Proc, vol. 1914, American Institute of Physics Inc.; 2017. doi: 10.1063/1.5016739.
[43] Darwis D, Mitomo H, Enjoji T, Yoshii F, Makuuchi K. Heat resistance of radiation crosslinked poly(ε-caprolactone). J Appl Polym Sci 1998;68:581–8. Doi: 10.1002/(SICI)1097-4628(19980425)68:4<581::AID-APP9>3.0.CO;2-I.
[44] Gedde UW. The Rubber Elastic State. Polym Phys, Dordrecht: Springer; 1999. p. 39–53. doi: 10.1007/978-94-011-0543-9_3.
[45] Mishra JK, Chang YW, Kim DK. Green thermoplastic elastomer based on polycaprolactone/epoxidized natural rubber blend as a heat shrinkable material. Mater Lett 2007;61:3551–4. https://doi.org/10.1016/j.matlet.2006.11.119.
[46] Takamura M, Nakamura T, Kawaguchi S, Takahashi T, Koyama K. Molecular characterization and crystallization behavior of peroxide-induced slightly crosslinked poly(L-lactide) during extrusion. Polym J 2010;42:600–8. https://doi.org/10.1038/pj.2010.42.
[47] Mishra JK, Chang YW, Kim W. The effect of peroxide crosslinking on thermal, mechanical, and rheological properties of polycaprolactone/epoxidized natural rubber blends. Polym Bull 2011;66:673–81. https://doi.org/10.1007/s00289-010-0376-9.
[48] Azizi Samir MAS, Alloin F, Sanchez JY, Dufresne A. Cellulose nanocrystals reinforced poly(oxyethylene). Polymer (Guildf) 2004;45:4149–57. https://doi.org/10.1016/j.polymer.2004.03.094.
[49] Castilla-Cortázar I, Vidaurre A, Marí B, Campillo-Fernández AJ. Morphology, crystallinity, and molecular weight of poly(ε-caprolactone)/graphene oxide hybrids. Polymers 2019;11. https://doi.org/10.3390/polym11071099.
[50] Kolahchi AR, Kontopoulou M. Chain extended poly(3-hydroxybutyrate) with improved rheological properties and thermal stability, through reactive modification in the melt state. Polym Degrad Stab 2015;121:222–9. https://doi.org/10.1016/j.polymdegradstab.2015.09.008.
[51] Khonakdar HA, Morshedian J, Wagenknecht U, Jafari SH. An investigation of chemical crosslinking effect on properties of high-density polyethylene. Polymer (Guildf) 2003;44:4301–9. https://doi.org/10.1016/S0032-3861(03)00363-X.
[52] Bhagabati P, Das D, Katiyar V. Bamboo-flour-filled cost-effective poly (ε-caprolactone) biocomposites: a potential contender for flexible cryo-packaging applications. Mater Adv 2021;2:280–91. https://doi.org/10.1039/d0ma00517g.